Available online at www.sciencedirect.com
ScienceDirect
Medical Engineering & Physics 31 (2009) 244–253
Medical Engineering & Physics
www.elsevier.com/locate/medengphy

Biomechanical comparison between lumbar disc arthroplasty and fusion

Shih-Hao Chen [a], Zheng-Cheng Zhong [b], Chen-Sheng Chen [c], Wen-Jer Chen [d], Chinghua Hung [b,*]

[a] *Department of Orthopaedics, Tzu Chi General Hospital, Taichung, Taiwan*
[b] *Department of Mechanical Engineering, National Chiao Tung University, 1001 Ta Hsueh Road, Hsinchu, Taiwan 300, ROC*
[c] *Department of Physical Therapy and Assistive Technology, National Yang Ming University, Taipei, Taiwan*
[d] *Department of Orthopaedics, Chang Gung Memorial Hospital, Taoyuan, Taiwan*

Received 5 November 2007; received in revised form 3 July 2008; accepted 16 July 2008

Abstract

The artificial disc is a mobile implant for degenerative disc replacement that attempts to lessen the degeneration of the adjacent elements. However, inconsistent biomechanical results for the neighboring elements have been reported in a number of studies. The present study used finite element (FE) analysis to explore the biomechanical differences at the surgical and both adjacent levels following artificial disc replacement and interbody fusion procedures.

First, a three-dimensional FE model of a five-level lumbar spine was established by the commercially available medical imaging software Amira 3.1.1, and FE software ANSYS 9.0. After validating the five-level intact (INT) model with previous *in vitro* studies, the L3/L4 level of the INT model was modified to either insert an artificial disc (ProDisc II; ADR) or incorporate bilateral posterior lumbar interbody fusion (PLIF) cages with a pedicle screw fixation system. All models were constrained at the bottom of the L5 vertebra and subjected to 150 N preload and 10 N m moments under four physiological motions.

The ADR model demonstrated higher range of motion (ROM), annulus stress, and facet contact pressure at the surgical level compared to the non-modified INT model. At both adjacent levels, ROM and annulus stress were similar to that of the INT model and varied less than 7%. In addition, the greatest displacement of posterior annulus occurred at the superior-lateral region. Conversely, the PLIF model showed less ROM, less annulus stress, and no facet contact pressure at the surgical level compared to the INT model. The adjacent levels had obviously high ROM, annulus stress, and facet contact pressure, especially at the adjacent L2/3 level.

In conclusion, the artificial disc replacement revealed no adjacent-level instability. However, instability was found at the surgical level, which might accelerate degeneration at the highly stressed annulus and facet joint. In contrast to disc replacement results, the posterior interbody fusion procedure revealed possibly accelerative degeneration of the annulus and facet joint at both adjacent levels.

Keywords: Finite element method; Artificial disc replacement; Lumbar interbody fusion; Adjacent segment degeneration

1. Introduction

The lumbar interbody fusion procedure is an effective and popular surgical technique for treating low back pain related to degenerative disc disease [1]. This procedure restores disc height, enlarges the stenotic foramen, stabilizes the spine, and provides mechanical strength between vertebrae. However, it has been argued that various spinal fusions restrain motion at the surgical level. This local environmental change at the surgical level results in high stress at the adjacent disc levels and accelerates degeneration. Patients may need to undergo another surgery for extended fusion at the adjacent levels. Clinical studies have reported incidence rates ranging from 6% to 58% [2–5]. Therefore, a non-fusion artificial disc was developed to solve the adjacent segment problems.

* Corresponding author. Tel.: +886 3 5712121x55160; fax: +886 3 5720634.
E-mail addresses: chhung@mail.nctu.edu.tw, zczhong2002@yahoo.com.tw (C. Hung).

1350-4533/$ – see front matter © 2008 IPEM. Published by Elsevier Ltd. All rights reserved.
doi:10.1016/j.medengphy.2008.07.007

The artificial disc is a mobile implant for degenerative disc replacement, which is designed to restore normal physiological motion and attempts to lessen the deterioration of the adjacent elements. Currently, two types of artificial disc, ball-and-socket and mobile core, are in the market. Prospective randomized clinical trials for the ball-and-socket type ProDisc II (Synthes, Inc., Paoli, PA/Spine Solutions, New York, NY) comparing the fusion device and disc arthroplasty under the Food and Drug Administration Investigational Device Exemption showed that this dynamic stabilizer was safe for use and had a good outcome [6–10].

Today, a number of finite element (FE) analyses and cadaver studies have attempted to evaluate the adjacent effects for artificial discs or to compare artificial discs with fusion. Goel et al. [11] found that the Charité slightly increased motion and facet loading at the implanted level compared to adjacent segments, while loadings at the adjacent levels decreased with use of a hybrid method. Grauer et al. [12] used a hybrid method to determine the effects of using the Charité artificial disc in a two-level disc replacement procedure compared to a single-level fusion plus a one-level artificial disc combination procedure. The changes at the adjacent non-operative levels were similar for both procedures (approximately 25%). Cunningham et al. [13] found that disc replacement, rather than pedicle instrumentation or Bagby and Kuslich (BAK) interbody instrumentation, preserved the kinematic properties and normal mapping of segment motion at the operative and adjacent intervertebral disc levels with identical load application. Denoziere and Ku [14] indicated that total disc replacement involves greater risk of instability and further degeneration at the surgical and lower adjacent levels than fusion procedure. Inconsistent results regarding the biomechanical effects of these spinal implants have been shown in previous studies. In addition, these studies lacked analysis of biomechanical differences at the surgical and adjacent discs and facet joints.

Therefore, the present study aimed to investigate the differences in the important biomechanical parameters between artificial disc replacement (ADR) and fusion by FE analysis on a five-segment spine model. A commonly used posterior lumbar interbody fusion (PLIF) model was chosen for this study because the use of additional posterior fixation points has generally resulted in small differences between cage types and approaches [15–19]. The main parameters studied were range of motion (ROM), facet contact pressure (FCP), maximum von Mises stress of the disc annulus, posterior displacement on the posterior annulus region (disc bulge), and contour of the stress distribution at the adjacent disc annulus.

2. Materials and methods

Three FE models of lumbar spine were constructed in the present study: The first model was of an intact lumbar spine; the other two models were of a lumbar spine implanted with a pair of Stryker cages (Stryker Orthopaedics, Mahwah, NJ, U.S.) and pedicle screw implant or of a lumbar spine with a ProDisc II artificial disc.

2.1. FE model of the intact lumbar spine (INT model)

To create a three-dimensional FE model, CT scan DICOM files of the L1–L5 lumbar spine of a middle-aged male were obtained at 1-mm intervals. The commercially available visualization software Amira 3.1.1 (Mercury Computer Systems, Inc., Berlin, Germany) was used to reconstruct three-dimensional surface geometry through sequential cross-section contours. Then, the Drawing eXchange Format (DXF) file was converted to the Initial Graphics Exchange Specification (IGES) file.

The FE analysis software ANSYS 9.0 (ANSYS Inc., Canonsburg, PA) was used to reconstruct the FE model by converting the IGES file to ANSYS Parametric Design Language (APDL) code. The INT model was an osteoligamentous lumbar spine, which included the vertebrae, intervertebral discs, endplates, posterior bony elements, and all seven ligaments.

The material properties of the INT model are listed in Table 1 and were chosen from previous studies [20–28]. All seven ligaments and collagen fibers were simulated by two-node link elements with resistance tension only, and they were arranged in the anatomical direction given by the textbook [29]; the cross-sectional area of each ligament was obtained from previous studies [20,25–27]. An eight-node solid element was used for modeling the cortical bone, cancellous bone, endplate, and annulus ground substance. Cortical bone and cancellous bone were assumed to be homogeneous and transversely isotropic [21]. The intervertebral disc consisted of annulus ground substance and nucleus pulposus, which embeds collagen fibers in the ground substance. The annulus ground substance was simulated by using a hyperelastic, two-parameter Mooney-Rivlin formulation [24]. In the radial direction, twelve double cross-linked fiber layers were defined, and those fibers were bounded by the annulus ground substance and both endplates. In addition, these fibers had decreased elastic strength proportionally, from the outermost layer to the innermost. Therefore, the collagen fibers in different annulus layers were weighted (elastic modulus at the outermost layers 1–3: 1.0, layers 4–6: 0.9, layers 7–9: 0.75, and at the innermost layers 10–12: 0.65; cross-sectional areas at the outermost layers 1–3: 1.0, layers 4–6: 0.78, layers 7–9: 0.62, and at the innermost layers 10–12: 0.47), and they were defined based on previous studies [25,30]. The nucleus pulposus was modeled as an incompressible fluid with bulk modulus of 1666.7 MPa by an eight-node fluid element [20,22]. The facet joint was treated as a sliding contact problem using surface-to-surface contact elements, and the coefficient of friction was set at 0.1 [30,31]. The initial gap between a pair of facet surfaces was possible within 0.5 mm.

Table 1
Material properties used in the FE model

Material	Element type	Young's modulus (MPa)	Poisson's ratio	Area (mm^2)	References
Bone	Solid	$E_x = 11300$	$\nu_{xy} = 0.484$	–	[21]
Cortical		$E_y = 11300$	$\nu_{xz} = 0.203$		
		$E_z = 22000$	$\nu_{yz} = 0.203$		
		$G_x = 3800$			
		$G_y = 5400$			
		$G_z = 5400$			
Cancellous	Solid	$E_x = 140$	$\nu_{xy} = 0.45$	–	[21]
		$E_y = 140$	$\nu_{xz} = 0.315$		
		$E_z = 200$	$\nu_{yz} = 0.315$		
		$G_x = 48.3$			
		$G_y = 48.3$			
		$G_z = 48.3$			
Posterior bone	Solid	3500	0.25	–	[20]
Disc					
Nucleus pulposus	Fluid	1666.7	–	–	[20,22]
Ground substance	Solid	$C_{10} = 0.42$	–	–	[24]
		$C_{01} = 0.105$			
Annulus fibers	Link				[25,30]
Outermost		550	–	0.76	
Second		495	–	0.5928	
Third		412.5	–	0.4712	
Innermost		357.5	–	0.3572	
Cartilaginous endplates	Solid	24	0.4	–	[20]
Ligaments	Link				[20,25–27]
ALL		7.8	–	24	
PLL		10	–	14.4	
TL		10	–	3.6	
LF		15	–	40	
ISL		10	–	26	
SSL		8	–	23	
CL		7.5	–	30	
Spinal instrumentation (titanium alloy)	Beam	110000	0.28	$D = 6$ mm	
Stryker O.I.V. cage (titanium alloy)	Solid	110000	0.28	–	
ProDisc II metallic endplate (CoCrMo alloy)	Solid	210000	0.3	–	
Polyethylene inlay (UHMWPE)	Solid	1016	0.46	–	[28]

ALL = anterior longitudinal ligament; PLL = posterior longitudinal ligament; TL = transverse ligament; LF = ligamentum flavum; ISL = interspinous ligament; SSL = supraspinous ligament; CL = capsular ligament.

The FE model of the intact lumbar spine consisted of 84,592 elements and 94,162 nodes (Fig. 1(a)).

2.2. FE model of the PLIF model

To simulate the PLIF model, the L3/L4 level of the INT model underwent laminectomy and partial discectomy, which included removal of supraspinous, interspinous, and flavum ligaments; then, bilateral titanium alloy cages (12 mm × 16 mm × 24 mm) with pedicle screw fixation were inserted. In this model, four pedicle screws ($r = 3$ mm) and two rods ($r = 3$ mm) were modeled with three-dimensional beam elements. The beam element was designed as a full constraint between the pedicle screws and vertebrae. Two titanium cages were placed between the vertebral bodies, and the bone–cage interface was modeled through surface-to-surface contact elements that were able to transmit compression forces, but not tension. The small teeth on the cage were neglected in our simulation; however, a higher coefficient of friction (0.8) was used in the contact interface to prevent cage slip motion [30]. The PLIF model consists of 181,081 elements and 104,035 nodes (Fig. 1(b)).

2.3. FE model of the anterior lumbar ADR model

To simulate the ADR model, a ProDisc II was implanted into the INT model at L3/L4. Following the standard surgical procedure, the nucleus was totally removed, and the anterior

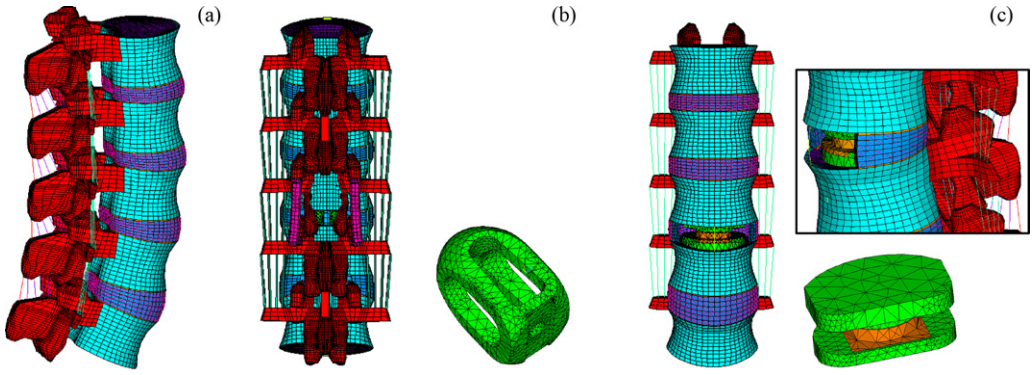

Fig. 1. FE model of the L1–L5 segments is shown: (a) intact; (b) with lumbar spine inserted bilateral titanium cages supplemented with pedicle screws at L3/L4; and (c) with lumbar spine implanted ProDisc II artificial disc at L3–L4.

longitudinal ligament was preserved. Only anterior and inner layers of the annulus were removed at the surgical level.

For simplification, the keel of the metallic plate surfaces was regarded as a flat surface. A perfect constraint was applied between the metallic plate and adjacent vertebrae. Deformable surface-to-surface contact behavior was modeled between the polyethylene inlay and the superior metallic plate, and the coefficient of friction for the polyethylene–CoCrMo alloy contact surface was chosen to be 0.07 [32]. The ADR model consists of 113,315 elements and 91,126 nodes (Fig. 1(c)).

2.4. Boundary and loading conditions

The loading condition was similar to the *in vitro* study of Yamamoto et al., in which the multi-level lumbar spine was subjected to the maximum possible load without causing spinal injury [33]. Therefore, all four physiological motions were imposed, each with a moment of 10 N m and a preload of 150 N on the superior surface of the L1 level. These models constrained all degrees of freedom at the inferior surfaces of the L5 vertebra.

3. Results

The results are reported at two levels of analysis. First, convergence test and model validation assessments are presented. Second, the biomechanical behavior of the lumbar spine with the PLIF model or the ADR model, respectively, is compared to that of the INT model. In our results, the data were normalized to the INT model as percentage values under each loading mode.

3.1. Convergence test and model validation results

In order to get reliable data, the convergence test and model were validated. For the convergence test, three mesh densities (4,750 elements/4,960 nodes, coarse mesh density model; 27,244 elements/30,630 nodes, normal mesh density model; and 84,594 elements/94,162 nodes, finest mesh density model) were selected to test for ROM changes in the INT model, and the finest mesh density was chosen since the change was within 1.03% (<0.2°). For the model validation, ROM in the five levels of the INT model was validated with previous cadaveric *in vitro* tests [31,33–35]. The current INT model showed stiffer behavior in flexion, and it had a ROM value that was four degrees less than that in Rohlmann's *in vitro* study. Otherwise, softer situations were obtained in extension and torsion as compared with the *in vitro* test data, but the differences were still within two degrees (Fig. 2). Overall, the discrepancy between the *in vitro* tests and our FE simulation was within one standard deviation [35]. A comparison of the torsion of the facet contact forces

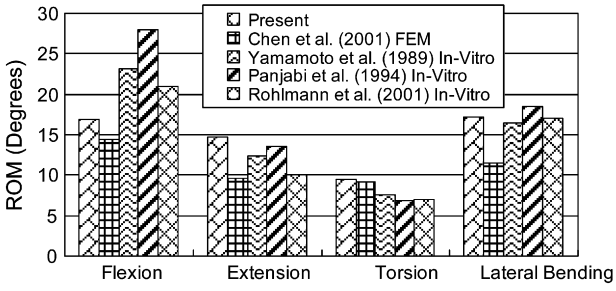

Fig. 2. ROM calculated for the five levels of intact lumbar spine is compared to previous *in vitro* experiments and analytical study.

Table 2
Listed is a comparison of torsion in total facet contact forces (N) between the present study and those of Chen and Shirazi-Adl

Torsion	Loading condition	L1–L2	L2–L3	L3–L4	L4–L5
Present study	10 N m with 150 N axial force	121	130	125	127
Chen et al.'s study (2001) [31]	10 N m with 150 N axial force	121	157	161	155
Shirazi-Adl's study (1994) [47]	10 N m	107	123	117	78

between the present INT model and that of Chen et al.'s [31] and that of Shirazi-Adl et al.'s [47] FE studies can be seen in Table 2. Our present FE study demonstrated lower contact forces than those using Chen's model. The present INT model was verified for further simulation.

3.2. Biomechanical analysis of three FE models

3.2.1. Comparison of ROM

For the ADR model, ROM at the surgical level increased by 9.2%, 81.1%, 67.9%, and 44.5% in flexion, extension, torsion, and lateral bending, respectively, compared to the INT model. The ROM varied less than 7% at both adjacent levels.

For the PLIF model, ROM at the surgical level decreased by 86.3%, 86.6%, 53.2%, and 78.2% in flexion, extension, torsion, and lateral bending, respectively, compared to the INT model. ROM at the adjacent L2/L3 level changed by +23%, +18.6%, −0.7%, and +5.7%, and, at the L4/L5 level, it changed by +6%, +12.1%, −2.9%, and +8.5% in flexion, extension, torsion, and lateral bending, respectively (Fig. 3).

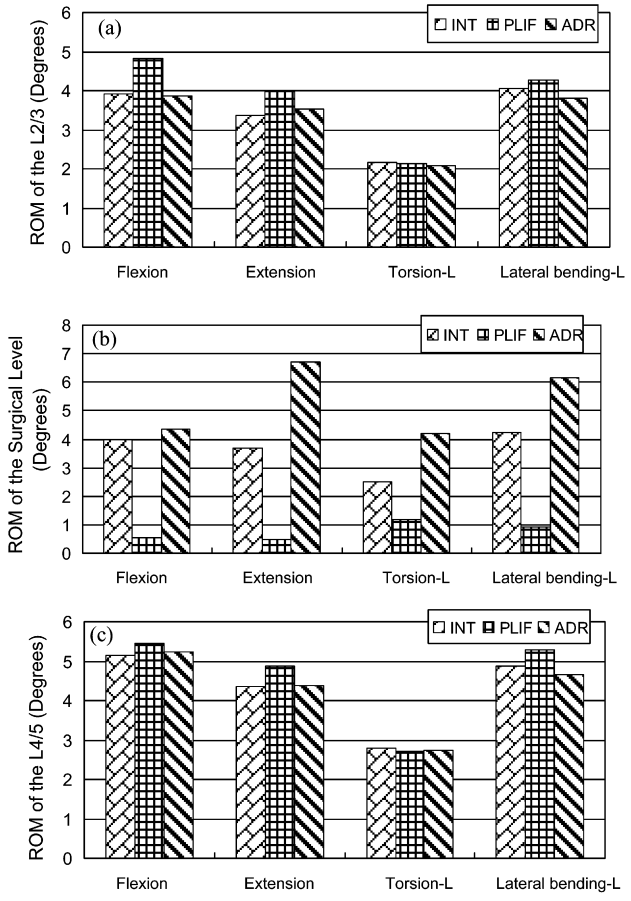

Fig. 3. ROM at the surgical and adjacent levels among the three FE models for different physiological motions is shown: (a) L2/L3 level; (b) surgical level; and (c) L4/L5 level.

3.2.2. von Mises stress in the disc annulus

For the ADR model, maximum annulus stress at the surgical level increased remarkably by 52.3%, 45.3%, 245.7%, and 59.3% in flexion, extension, torsion, and lateral bending, respectively, compared to the INT model. The annulus stress also varied within 7% at both adjacent levels, which were −0.3%, +6.9%, −4.6%, and −4.1% at L2/L3, and +2.2%, −1.4%, +6.4%, and −4.9% at L4/L5 in flexion, extension, torsion, and lateral bending, respectively, compared to the INT model.

For the PLIF model, the maximum annulus stress at the surgical level decreased remarkably by −84.6%, −78.2%, −48.2%, and −74.4% in flexion, extension, torsion, and lateral bending, respectively, compared to the INT model. The annulus stress increased at the adjacent L2/L3 level by 20.5%, 44.6%, 2.2%, and 4.2%, and at the adjacent L4/L5 level by 10.2%, 8.2%, 9.8%, and 12.2% in flexion, extension, torsion, and lateral bending, respectively (Fig. 4).

Moreover, the stress concentration and distribution pattern changed more obviously at the L2/3 annulus in the PLIF model: The solid arrows (Fig. 5) indicate that annulus stress during flexion (Panel A) was concentrated at the anterior and posterior of the annulus regions close to both sides of the endplate; during extension (Panel B), it was concentrated at the posterior of the annulus regions close to the inferior side of the endplate; during torsion (Panel C), it was concentrated

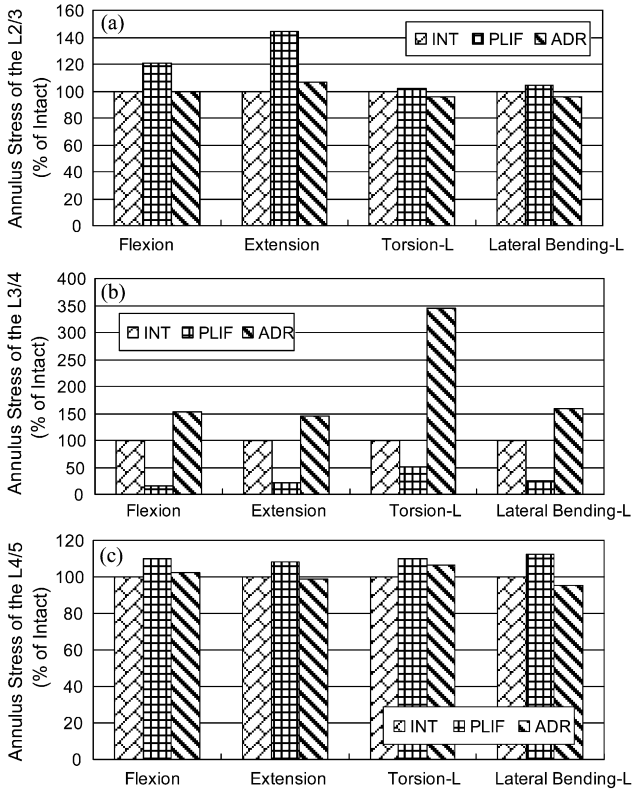

Fig. 4. von Mises stresses of the disc annulus are compared among the three FE models for the different physiological motions; (a) L2/L3 level; (b) surgical level; and (c) L4/L5 level.

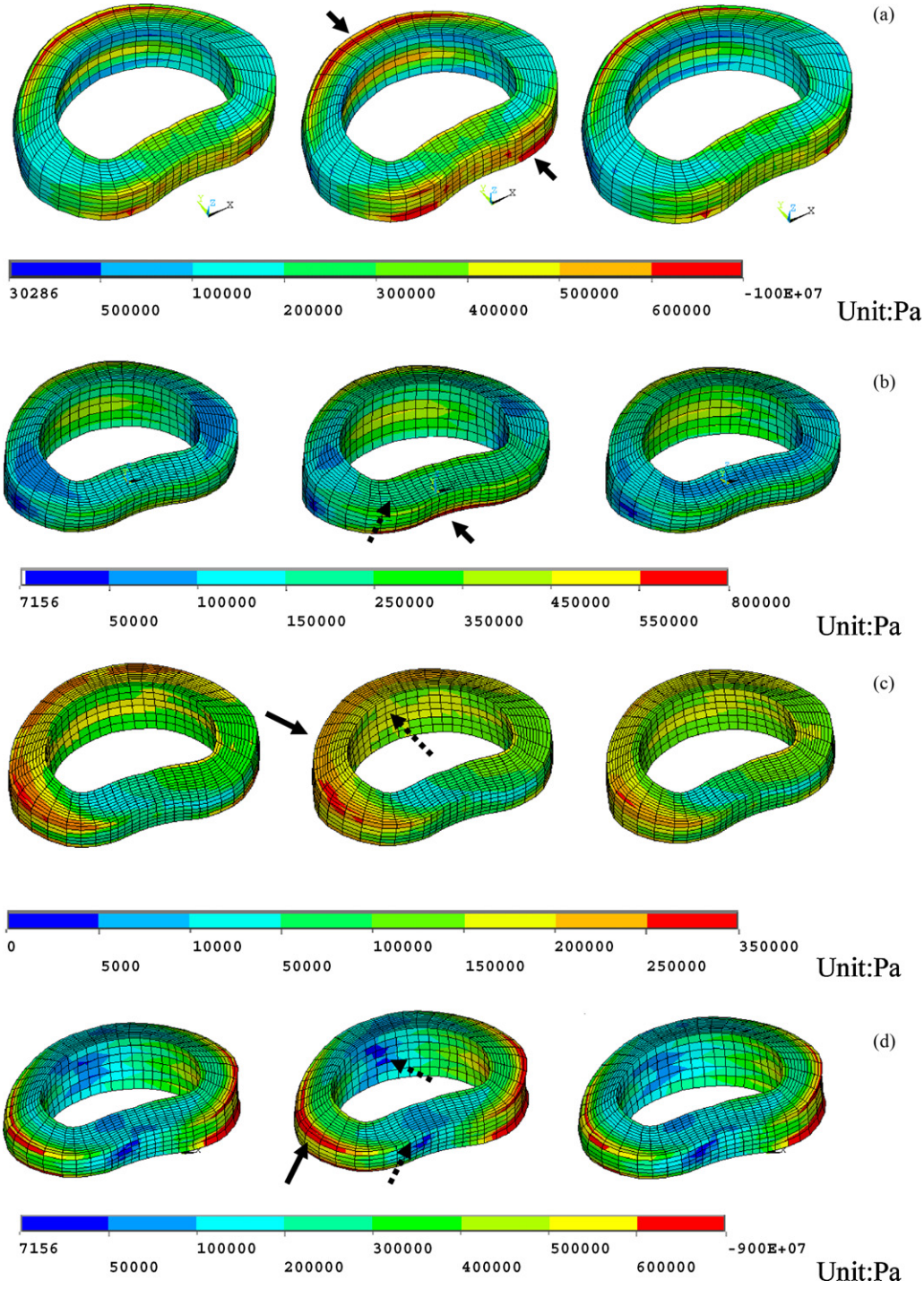

Fig. 5. The von Mises stress distribution of the L2/L3 adjacent disc annulus under four physiological motions is depicted for (a) flexion model; (b) extension model; (c) torsion model; and (d) lateral bending model (Left: INT; Middle: PLIF; Right: ADR). The solid arrows indicate stress concentration regions. The dotted arrows indicate the regions where the stress distribution pattern changed.

at the circumferential ring of the annulus regions close to the endplate; and, during lateral bending (Panel D), it was concentrated at the left side regions close to the endplate. The dotted arrows (Fig. 5) indicate that the stress distribution pattern changed. For the ADR model, the stress concentration at the L2/3 level was not obvious, and the stress pattern was close to that of the INT model; however, the stress distributions at the L2/3 annulus in extension were dissimilar to the INT.

3.2.3. *Comparison of FCP*

For the ADR model, the right side FCP at surgical level for left torsion demonstrated a 5.6-fold magnitude increase

Table 3
Facet contact pressure at the surgical and adjacent levels under extension and left torsion (% of intact) is listed

Motion	Model	Level		
		L2/3	L3/4	L4/5
Left or right side facet contact pressure under extension (% of intact)	PLIF	191.3	0	134
	ADR	121.5	109.3	100.3
Right side facet contact pressure under left torsion (% of intact)	PLIF	105.3	2.7	122.1
	ADR	101.2	663.9	104.6

compared to the INT model and FCP at the L2/3 adjacent level for extension demonstrated a 21.5% increase, which was similar to torsion in the INT model for both adjacent levels (within 5%).

For the PLIF model, minimal FCP was observed at the surgical level in left torsion and extension due to the load shearing of the implanted pedicle screws. For extension, FCP at both adjacent levels increased markedly by 91.3% at L2/3 and 34% at L4/5 compared to the INT model; for left torsion, the right side FCP increased by 5.3% at L2/L3 and 22.1% at L4/L5 compared to the INT model (Table 3).

Therefore, the effect of FCP was emphasized at the surgical level in torsion following insertion of a replacement artificial disc. In contrast, FCP increased obviously at the adjacent levels in extension following implantation of fusion cages.

3.2.4. Changes in displacement of the posterior annulus regions at the surgical level

The displacement values of the posterior annulus were calculated from nodal deformation in the anterior–posterior direction for the INT and the ADR models (the posterior annulus of the PLIF model was removed). In this study, displacements at three regions of the posterior annulus (U for upper; M for middle; and L for lower) are shown in Fig. 6. As compared to the INT model, displacement at the posterior annulus of the ADR model had higher values in all motions. The greatest displacement occurred at the posterior–lateral annulus; the data, shown in Fig. 6, are as follows: U:M:L is 6.43:5.91:5.09 mm in flexion (point 17), 5.48:4.79:4.12 mm in extension (point 16), 2.67:2.09:1.55 mm in left torsion (point 1), and 0.42:0.42:0.22 mm in left lateral bending (point 1). Therefore, the highest values in displacement were found in the upper region of the posterior–lateral annulus.

4. Discussion

It is known from previous clinical reports that spinal fusion plus pedicle screw instrumentation demonstrates good stability at the surgical level, but it also demonstrates high incidences of accelerative disc degeneration and facet joint arthritis at the adjacent levels [2,4,36,37]. In the present study, the PLIF model demonstrated low ROM, low annulus stress, and almost no FCP at the surgical level compared to the INT model. However, higher ROM, annulus stress, and FCP, especially in flexion and extension, were observed at the adjacent upper levels using the load-controlled method. Goel et al. [11,12] indicated that, in real life, people bend their spines within a similar, limited ROM regardless of whether their spine is healthy or has undergone spinal surgery. Therefore, it is recommended that true physiological conditions should be obtained by applying different moments so that the same overall ROMs are achieved for both intact and implant models. Thus, the hybrid method (ROM-controlled method) might be more clinically relevant and might result in greater ROM at adjacent levels. In our primary simulation data using the ROM-controlled method, the trends at the adjacent levels were similar to those of the load-controlled method; however, ROM at adjacent levels in the ROM-controlled method increased much more than in the load-controlled method [38]. Therefore, the results from the present FE model demonstrated a similar trend to the clinical findings and could still explain adjacent-level effects.

The surgical principles in total disc replacement are to restore normal physiological motion and to avoid disc degeneration at adjacent levels. Unlike the traditional fusion technique, total disc replacement has shown inconsistent results in clinical reports concerning accelerative degeneration at the surgical and adjacent levels. For example, the ProDisc used in the lumbar spine increased ROM at the surgical level in some studies [8,39], but opposing findings have also been reported [40]. van Ooij et al. [41] indicated that the complications following implantation of a mobile core artificial disc included degeneration of the facet joint at the surgical level and disc degeneration at the adjacent level. Shim et al. [42] compared the three-year clinical follow-up outcomes of Charité and ProDisc replacements and found that, for both groups, 32% of the facet joints at the surgical level and 28.6% of the discs at the adjacent level showed an aggravation of degeneration. However, Siepe [9] and Tropiano's data [10] demonstrated no disc degenerative changes at the level adjacent to the disc replacement and reported only a few facet joint problems. These conflicting results may be due to many factors, such as size of the implant, patient selection, multi-level replacements, evaluation method, malalignment of implant, length of follow-up period, imprecise diagnostic criteria, various biologic change, and technical errors during surgery. To assess these complex factors, a FE analysis adhering to a standard surgical procedure evaluated biomechanical changes at surgical and adjacent levels. In the present simulation, the ADR model demonstrated greater ROM, increased

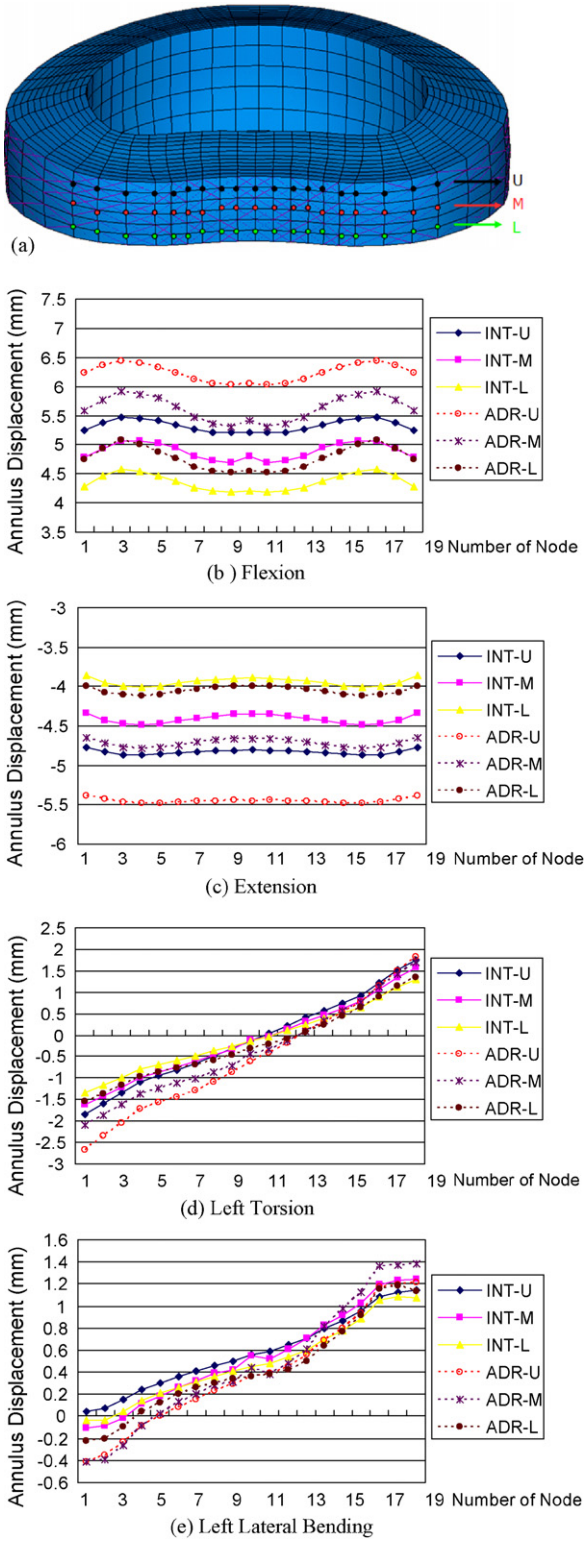

Fig. 6. Displacement changes in the posterior disc annulus at the surgical level are shown: (a) nodal deformation of the spots on the U, M, and, L regions are shown (U for upper; M for middle; and L for lower). The node at the leftmost side is number one, and the node at rightmost side is number nineteen. (b) Flexion, (c) extension, (d) left torsion, and (e) left lateral bending. In the figure, the positive value indicates that the annulus was displaced toward the anterior, while the negative value indicates that the annulus was displaced toward the posterior.

stress on the remaining annulus, and greater FCP at the surgical level than the INT model. No obvious differences existed at adjacent levels between the ADR model and the INT model. Therefore, the present results support an increased likelihood of accelerative degeneration of the discs and facets occurring at the surgical level and a reduced possibility of adjacent-level problems following total disc replacement.

The present study, incorporating a five-level FE lumbar spine model simulating all four physiological loading modes, demonstrated that the ADR could not restore normal physiological motion and caused instability at the surgical level in extension, torsion, and lateral bending. The ROM for extension post ProDisc implantation increased 81%, indicating instability. This particular result is in agreement with findings from most previous studies [11,23]. Several reports show that the remaining annulus at the surgical level plays an important role in providing stability [23,43]. In the present results, stress on the remaining annulus at the ADR level was remarkably high under all four motions, especially under torsion, while annulus stress at the adjacent levels was similar to the INT model. Instability and high annulus stress at the surgical level might induce degeneration at the remaining annulus following long-term use; consequently, shear and compression force might impose on the implant and induce disc height loss, inlay dislocation, polyethylene wear, or implant subsidence [42,44]. To retard possible degeneration, patients should avoid high external loading under all physiological motions as normal activities are resumed post surgery.

In addition, the greatest annulus displacement occurred in the upper region of the posterior–lateral annulus in the ADR model. Total disc replacement might induce annulus tear and bulging at this area under extension, torsion, and lateral bending following ProDisc implantation. The long-term effect at this weak point should be observed clinically. Huang et al. [45] indicated that an artificial disc with a constraint design offers a facet-protective effect by decreasing facet loads under extension. In our simulation, the FCP increased only 9% at the surgical level under extension, which is in agreement with Huang's report. However, there was an obvious 5.6-fold increase in FCP under torsion load at the surgical level, which might accelerate degeneration. The constraint design of the ProDisc limits motion only under flexion–extension and lateral bending, but not under torsion. Therefore, a new artificial disc design is required to constrain torsional motion and avoid high FCP.

For the adjacent levels with the artificial disc, there was no difference in ROM, annulus stress, or FCP under the four physiological motions. Our FE analysis results are in agreement with previous biomechanical studies [23,46]. However, opposing results have been reported: In Denoziere and Ku's [14] study, artificial disc replacement showed a greater risk of instability and of further degeneration than did fusion at the adjacent levels. The differences across these studies might be attributed to different loading conditions studied, number of spinal segments studied, and specific adjacent level analyzed (only the lower level; L4/5). Based on our simulation, it is

concluded that accelerated degeneration would not occur at the adjacent discs and facet joints following implantation of a ProDisc.

After implanting spinal cages the stress on the adjacent disc annulus increased remarkably and concentrated at the outermost layers close to the endplate regions; this stress distribution pattern was dissimilar to the intact model, as shown with arrows in Fig. 5, which might be related to adjacent disc degeneration at the interface between the annulus and endplate.

Several of the limitations of this study are related to the slightly simplified and idealized material properties of this simulation, such as the nonlinear behavior of the spinal ligaments, the viscoelasticity of the disc, and the grade of degenerative disc, which differ from those of a cadaver specimen. Degenerative disc is common in most patients before surgery, and difficulty in modeling the various grades and complexities of degeneration in a disc, such as delamination, dehydration, or reduced disc height, prohibits obtaining the unique material properties for each or even a general degenerative disc situation. Therefore, normal material properties were used in our simulation. Also, the constrained behavior used in the bone-screw interface, the keel in the metallic plates of the ProDisc, and the bone ingrowth into the cage were also simplified. Pretension typically occurs following insertion of the ADR, which might distract the remaining annulus and reduce the ROM and facet loading at the surgical level, but this mechanism was not modeled here. The loading conditions of the present FE simulations were similar to those of the *in vitro* test; thus, the muscle contraction, complicated external load conditions, and pelvic movement were not considered in the present study. Several other studies have pointed out that displacement control or hybrid control is a better loading condition under which to predict adjacent-level effects on non-fusion spinal implants [11,46]. In the present study, only the traditional load-controlled method was of concern; therefore, the load- and displacement-controlled FE analyses of fusion and non-fusion spinal implants will be reported in the near future.

5. Conclusions

The artificial disc replacement demonstrated no adjacent instability; however, it did suggest surgical level instability, which could accelerate possible degeneration at the highly stressed annulus and facet joint. However, the traditional interbody fusion procedure revealed adjacent instability on the upper level, especially in flexion and extension, which might relate to a higher incidence of degeneration of the annulus and facet joint above the fusion level.

Acknowledgements

The present research was made possible through grants from the National Science Council (NSC94-2320-B-182-054), Taiwan. Simulations were partly performed at the National Center for High-performance Computing. We thank Professor CL Lin (Department of Mechanical Engineering, Chang Gung University) for his support in the licensing of Amira 3.1.

Conflict of interest

No benefits in any form have been or will be received from a commercial party related directly or indirectly to the subject of this manuscript.

References

[1] Fritzell P, et al. Lumbar fusion versus nonsurgical treatment for chronic low back pain—a multicenter randomized controlled trial from the Swedish lumbar spine study group. Spine 2001;26(23):2521–34.
[2] Lee CK. Accelerated degeneration of the segment adjacent to a lumbar fusion. Spine 1988;13:375–7.
[3] Lehmann TR, Spratt KF, Tozzi JE, Weinstein JN, Reinarz SJ, El-Khoury GY, et al. Long-term follow-up of lower lumbar fusion patients. Spine 1987;12:97–104.
[4] Rahm MD, Hall BB. Adjacent segment degeneration after lumbar fusion with instrumentation: a retrospective study. J Spinal Disord 1996;9:392–400.
[5] Kuslich SD, Danielson G, Dowdle JD, Sherman J, Fredrickson B, Yuan H, et al. Four-year follow-up results of lumbar spine arthrodesis using the Bagby and Kuslich lumbar fusion cage. Spine 2000;25:2656–62.
[6] McAfee PC, Polly DW, Cunningham B, Gaines B, Hallab N, Lubicky J, et al. Clinical summary statement. Spine 2003;28:S196–8.
[7] Zigler JE. Clinical results with ProDisc: European experience and U.S. investigation device exemption study. Spine 2003;28:S163–6.
[8] Delamarter RB, Fribourg DM, Kanim LEA, Bae H. ProDisc artificial total lumbar disc replacement: introduction and early results from the United States clinical trial. Spine 2003;28:S167–75.
[9] Siepe CJ, Mayer HM, Wiechert K. Clinical results of total lumbar disc replacement with ProDic II: three-year results for different indications. Spine 2006;31:1923–32.
[10] Tropiano P, Huang RC, Girardi FP, Marney T. Lumbar disc replacement: preliminary results with ProDisc II after a minimum follow-up period of 1 year. J Spinal Disord Tech 2003;16(4):362–8.
[11] Goel VK, Grauer JN, Patel TCh, Biyani A, Sairyo K, Vishnubhotla S, et al. Effects of Charité artificial disc on the implanted and adjacent spinal segments mechanics using a hybrid testing protocol. Spine 2005;30:2755–69.
[12] Grauer JN, Biyani A, Faizan A, Kiapour A, Sairyo K, Ivanov A, et al. Biomechanics of two-level Charite artificial disc placement in comparison to fusion plus single-level disc placement combination. Spine J 2006;6:659–66.
[13] Cunningham BW, Gordon JD, Dmitriev AE, Hu N, McAfee PC. Biomechanical evaluation of total disc replacement arthroplasty: an in vitro human cadaveric model. Spine 2003;28:S110–7.
[14] Denoziere G, Ku DN. Biomechanical comparison between fusion of two vertebrae and implantation of an artificial intervertebral disc. J Biomech 2006;39:766–75.
[15] Oxland TR, Lund T. Biomechanics of stand-alone cages and cages in combination with posterior fixation: a literature review. Eur Spine J 2000;9(Suppl 1):s95–101.
[16] Lund T, Oxland TR, Jost B, Cripton P, Grassmann S, Etter C, et al. Interbody cage stabilization in the lumbar spine: biomechanical evaluation of cage design, posterior instrumentation and bone density. J Bone Joint Surg (Br) 1998;80:351–9.

[17] Wang ST, Goel VK, Fu CY, Kubo S, Choi W, Liu CL, et al. Posterior instrumentation reduces differences in spine stability as a result of different cage orientations: an in vitro study. Spine 2005;30: 62–7.
[18] Hitchon PW, Goel V, Rogge T, Dooris A, Drake J, Torner J. Spinal stability with anterior or posterior ray threaded fusion cages. J Neurosurg 2000;93:102–8.
[19] Voor MJ, Mehta S, Wang M, Zhang YM, Mahan J, Johnson JR. Biomechanical evaluation of posterior and anterior lumbar interbody fusion techniques. J Spinal Disorder 1998;11:328–34.
[20] Goel VK, Monroe BT, Gilbertson LG, Brinckmann P. Interlaminar shear stresses and laminae separation in a disc. Finite element analysis of the L3–L4 motion segment subjected to axial compressive loads. Spine 1995;20:689–98.
[21] Lu YM, Hutton WC, Gharpuray VM. Do bending, twisting, and diurnal fluid change in the disc affect the propensity to prolapse? A viscoelastic finite element model. Spine 1996;21:2570–9.
[22] Rohlmann A, Zander T, Bergmann G. Effects of fusion-bone stiffness on the mechanical behavior of the lumbar spine after vertebral body replacement. Clin Biomech 2006;21:221–7.
[23] Rohlmann A, Zander T, Bergmann G. Effects of total disc replacement with ProDisc on intersegmental rotation of the lumbar spine. Spine 2005;30:738–43.
[24] Schmidt H, Heuer F, Simon U, Kettler A, Rohlmann A, Claes L, et al. Application of a new calibration method for a three-dimensional finite element model of a human lumbar annulus fibrosus. Clin Biomech 2006;21:337–44.
[25] Shirazi-Adl A, Ahmed AM, Shrivastava SC. Mechanical response of a lumbar motion segment in axial torque alone and combined with compression. Spine 1986;11:914–27.
[26] White 3rd AA, Panjabi MM. Clinical biomechanics of the spine. 2nd ed. Philadelphia/Toronto: J.B. Lippincott Company; 1990.
[27] Lee KK, Teo EC, Fuss FK, Vanneuville V, Qiu TX, Ng HW, et al. Finite-element analysis for lumbar interbody fusion under axial loading. IEEE Trans Biomed Eng 2004;51:393–400.
[28] Liau JJ, Hu CC, Cheng CK, Huang CH, Lo WH. The inference of inserting a Fuji pressure sensitive film between the tibiofemoral joint of knee prosthesis on actual characteristics. Clin Biomech 2001;16: 160–6.
[29] Agur AMR, Lee MJ. Grant's atlas of anatomy. 10th ed. Philadelphia: Lippincott Williams & Wilkins; 1999.
[30] Polikeit A, Ferguson SJ, Nolte LP, Orr TE. Factors influencing stresses in the lumbar spine after the insertion of intervertebral cages: finite element analysis. Eur Spine J 2003;12:413–20.
[31] Chen CS, Cheng CK, Liu CL, Lo WH. Stress analysis of the disc adjacent fusion in lumbar spine. Med Eng Phys 2001;23:483–91.
[32] Godest AC, Beaugonin M, Haug E, Taylor M, Gergson PJ. Simulation of a knee joint replacement during a gait cycle using explicit finite element analysis. J Biomech 2002;35:267–75.
[33] Yamamoto I, Panjabi MM, Crisco T, Oxland T. Three-dimension movement of the whole lumbar spine and lumbosacral joint. Spine 1989;14:1256–60.
[34] Panjabi MM, Oxland TR, Yamamoto I, Crisco JJ. Mechanical behavior of the human lumbar and lumbosacral spine as shown by three-dimensional load–displacement curves. J Bone Joint Surg Am 1994;76:413–24.
[35] Rohlmann A, Neller S, Claes L, Bergmann G, Wilke HJ. Influence of a follower load on intradiscal pressure and intersegmental rotation of the lumbar spine. Spine 2001;26:E557–61.
[36] Etebar S, Cahill DW. Risk fractures for adjacent segment failure following lumbar fixation with rigid instrumentation for degenerative instability. J Neurosurg 1999;90:163–9.
[37] Aota Y, Kumano K, Hirabayashi S. Post-fusion instability at the adjacent segments after rigid pedicle screw fixation for degenerative lumbar spinal disorders. J Spinal Disord 1995;8:464–73.
[38] Zhong ZC, Chen SH, Chen WJ, Hung C. Comparison of the load and displacement controlled finite element analyses on fusion and non-fusion spinal implants. J Biomech 2007;40(S2):S353.
[39] Zigler JE. Lumbar spine arthroplasty using the ProDisc II. Spine J 2004;4:S260–7.
[40] Leivseth G, Braaten S, Frobin W, Brinckmann P. Mobility of lumbar segments instrumented with a ProDisc II prosthesis: a two-year follow-up study. Spine 2006;31:1726–33.
[41] van Ooij A, Cumhur Oner F, Verbout ABJ. Complications of artificial disc replacement: a report of 27 patients with the SB Charité disc. J Spinal Disord Techn 2003;16:369–83.
[42] Shim CS, Lee SH, Shin HD, Kang HS, Choi WC, Jung B, et al. Charité versus ProDisc: a comparative study of a minimum 3-year follow-up. Spine 2007;32:1012–8.
[43] Dooris AP, Goel VK, Grodland NM, Gilbertson LG, Wilder DG. Load-sharing between anterior and posterior elements in a lumbar motion segment implanted with an artificial disc. Spine 2001;26:E122–9.
[44] Kurtz SM, van Ooij A, Ross R, de Waal Malefijt J, Peloza J, Ciccarelli L, et al. Polyethylene wear and rim fracture in total disc arthroplasty. Spine J 2007;7:12–21.
[45] Huang RC, Girardi FP, Gammisa GF, Wright TM. The implications of constraint in lumbar total disc replacement. J Spinal Disord 2003;16(4):412–7.
[46] Panjabi MM, Henderson G, Abjornson C, Yue J. Multidirectional testing of one- and two-level ProDisc-L versus simulated fusions. Spine 2007;32:1311–9.
[47] Shirazdi-Adl A. Nonlinear stress analysis of the whole lumbar spine in torsion-mechanics of facet articulation. J Biomech 1994;27:289–99.